Biosensors and Bioelectronics 132 (2019) 302–309

Contents lists available at ScienceDirect

Biosensors and Bioelectronics

journal homepage: www.elsevier.com/locate/bios

Trimetallic signal amplification aptasensor for TSP-1 detection based on Ce-MOF@Au and AuPtRu nanocomposites

Xiaoxue Fu[a,1], Junlin He[b,1], Chengli Zhang[c], Jun Chen[a], Yilin Wen[a], Jia li[a], Weiran Mao[a], Hangtian Zhong[b], Jiahao Wu[b], Xingduo Ji[b], Chao Yu[a,b,c,*]

[a] College of Pharmacy, Chongqing Medical University, Chongqing 400016, PR China
[b] School of Public Health, Chongqing Medical University, Chongqing 400016, PR China
[c] Institute of Life Science, Chongqing Medical University, Chongqing 400016, PR China

ARTICLE INFO

Keywords:
Thrombospondin-1
Ce-based metal-organic framework
Trimetallic nanocomposite
Electrochemical aptasensor

ABSTRACT

In this work, an aptamer was used as the target capturing agent and a trimetallic signal amplification strategy based on Ce-MOF@Au and AuPtRu NPs was demonstrated for the sensitive detection of TSP-1. Herein, the synthesized AuPtRu nanocomposite (AuPtRu NPs) not only acts as the catalyst for catalyzing hydrogen peroxide but also acts as a nanocarrier for capturing the -NH_2 termination single strand DNA (S1) to obtain the signal probe (SP, AuPtRu nanocomposite/S1). Then, SP was efficiently linked into TSP-1 aptamers with the addition of complementary linking strands to form M1 (SP/aptamer). The Ce-MOF@Au nanocomposites were obtained by in situ reduction and used as GCE electrode modification materials. The -NH_2-modified capture probe (CP) DNA was immobilized on the surface of Ce-MOF@Au nanocomposites for hybridizing SP. In the presence of the target TSP-1, the aptamer recognizes the target and binds strongly so that SP is released from the prepared M1 and then hybridized with CP. When the detection solution contains an electrochemical matrix of H_2O_2, AuPtRu NPs can oxidize H_2O_2 to obtain an enhanced signal. Furthermore, the proposed aptasensor has a very low LOD of 0.13 fg mL^{-1} TSP-1 in the detection range of 1 fg mL^{-1} to 10 ng mL^{-1}. Moreover, the proposed platform also has application implications for other potential targets.

1. Introduction

Cardiovascular disease (CVD), one of the leading causes of death worldwide, may present an increase in the level of biomarker molecules in the blood. Identifying the biomarkers of the highest risk of CVDs for auxiliary diagnosis can prevent premature deaths (Nguyen et al., 2018; Yusuf et al., 2001). Thrombospondin-1 (TSP-1), a promising candidate biomarker for CVD (Ji et al., 2014; Salajegheh, 2016), is expressed at higher levels in large atherosclerotic lesions and myocardial infarction (Chavez et al., 2012). Therefore, a series of methods such as tetrazolium salt colorimetry, and enzyme-linked immunosorbent assay (ELISA) have been developed for detecting TSP-1. However, all of these methods require complex treatment of the target samples. Thus, the sensitive and selective detection of TSP-1 in clinical samples remains challenging. Due to their extremely low limits of detection and potential for in situ analysis (Li et al., 2016), electrochemical sensors have enabled the realization of highly sensitive miniaturized platforms for TSP-1detection in CVDs diagnosis.

In recent years, metal-organic frameworks (MOFs), which are novel microporous materials with metal ions as nodes and organic ligands as linkers, have gradually attracted research attention (Dang et al., 2017). MOFs exhibit tunable sizes and morphologies (Li et al., 2015; Zhang et al., 2016) with properties of high pore volume, satisfactory electrochemical stability and easy modification (Campbell et al., 2015; Cui et al., 2016). Inspired by MOFs properties, Ce-based MOF (Ce-MOF) were synthesized in this work that not only inherit the advantages of traditional MOFs but also show strong adsorption capacity and good biocompatibility (Shen et al., 2016). The advantages of Ce-MOF indicate that Ce-MOF is highly suitable for use as electrode modification materials. The synthesis of Ce-MOF with benzenetricarboxylic acid as the organic framework has high efficiency and simple steps which will undoubtedly increase the feasibility of sensor construction (Xiong et al., 2015). In order to increase the conductivity of the electrode and to immobilize biomolecules, gold nanoparticles (Au NPs) are introduced to the surface of the Ce-MOF to form Ce-MOF@Au. In this design, the capture probe (CP) is immobilized on Ce-MOF@Au by Au-NH_2 bond to

* Correspondence to: College of Pharmacy, Chongqing Medical University, Box 380#, 1 Yi Xue Yuan Road, Chongqing 400016, PR China.
E-mail address: yuchaom@163.com (C. Yu).
[1] Junlin He and Xiaoxue Fu contributed equally to this work.

https://doi.org/10.1016/j.bios.2019.02.054
Received 28 September 2018; Received in revised form 14 February 2019; Accepted 18 February 2019
Available online 04 March 2019
0956-5663/ © 2019 Elsevier B.V. All rights reserved.

identify the signal probe. In our previous work, we have found that the use of reducing agents to reduce Au NPs in situ to carrier surface is prone to aggregation, making the synthesis method extremely limited. To solve this problem, in this work, polyvinyl pyrrolidone (PVP) was used as a protective agent to successfully avoid the aggregation of Au NPs (Xiao et al., 2012). It is well known that PVP is one of the attractive polymers for immobilizing metal nanoparticles. It has been reported that PVP molecules can be adsorbed on the growing precious metal core as a typical surfactant while preventing the aggregation of noble metal nanoparticles. (Chuanfu et al., 2012; Wang et al., 2010) To the best of our knowledge, the present work is the first exploration of a one-step synthesis method for reducing Au NPs in situ to the Ce-MOF surface to form robust nanocomposites (Ce-MOF@Au) for use as an electrode modification material.

To overcome the shortcoming of the instability of the biological recognition molecules (e.g., enzymes, antibodies) that has limited the biosensors from being used as much as anticipated, aptamers have been increasingly used in various sensing platforms due to their unique characteristics of high affinity and specificity to a wide variety of targets ranging from small molecules to large proteins (Bai et al., 2017; You et al., 2018). Aptamers are short synthetic nucleotide sequences obtained by an in vitro procedure from the cell SELEX (Ji et al., 2014). In addition to their affinity to targets, aptamers have advantages such as easy production, low-cost synthesis, high thermal stability, and ease of labeling and modification. They can also be easily immobilized on different surfaces with various chemistries (Du et al., 2010; Feng et al., 2011). Hence, aptamers should be applied as specific recognition components in various sensors as alternatives to antibodies. We aim to design an aptasensor that couples the specificity of an aptamer with a signal amplification mechanism for TSP-1 detection.

To achieve sensitive detection of trace substances, secondary signal substances are generally used to amplify the electrochemical response in the electrochemical sensor analysis technology (Zeng et al., 2015). Platinum (Pt) nanoparticles have long been known to have good catalytic performance. Rational design of the composition and structure is essential for designing highly active platinum catalysts (Eid et al., 2015; Gao et al., 2016). A growing variety of Pt trimetallic materials have been synthesized, such as FePtCu (Zhu et al., 2013), AuPdPt (Kang et al., 2013) and PtPdTe (Li et al., 2013) that have catalytic properties superior to Pt and Pt-based bimetallic materials. Ruthenium (Ru) is very stable and can be used as an excellent catalyst (Hong et al., 2015). Moreover, Ru is an effective hardener for platinum that can be used to increase the stability and catalytic properties of platinum (Christensen et al., 2010). Au NPs are widely used in electrochemical signal materials due to their high chemical stability and excellent biocompatibility (Pei et al., 2018; Tang et al., 2018). Therefore, combining the advantages of Au NPs, Pt NPs and Ru NPs, AuPtRu NPs were designed and synthesized for the first time in this work. AuPtRu NPs showed excellent stability, catalytic properties and ability to immobilize biomolecules. Briefly, the signal is greatly amplified by the synergistic catalysis of H_2O_2 by AuPtRu NPs.

To construct a multielement, synergistic nanosensing interface, a nucleic acid single strand 1 (S1) with a modified -NH_2 at the 5′ end was designed to react with an aptamer to form a double strand in a PCR machine. Then, S1 is linked to the signal material AuPtRu NPs via Au-NH_2 bond and Pt-NH_2 bond to form a signal probe (SP). In the presence of TSP-1, TSP-1 binds to the aptamer and induces the release of SP from the SP + aptamer double strand (M1). Meanwhile, the -NH_2 modified capture probe (CP) was immobilized on the electrode modified by Ce-MOF@Au. When CP recognizes the released SP and captures them, a large electrical signal is generated by the AuPtRu catalysis of H_2O_2. Due to the excellent conductivity of Ce-MOF@Au and the superior catalytic capability of AuPtRu NPs, the new technology platform achieves sensitive detection for TSP-1 in serum. We demonstrated that the proposed aptasensor has good prospects for applications in clinical research.

2. Experimental

2.1. Materials and reagents

Cerium(III) nitrate hexahydrate ($Ce(NO_3)_3{\cdot}6H_2O$), chloroplatinic acid ($H_2PtCl_6{\cdot}6H_2O$), potassium ferrocyanide ($K_4Fe(CN)_6$), potassium ferricyanide ($K_3Fe(CN)_6$) and Pluronic® F-127 were supplied by Sigma-Aldrich (St. Louis, USA, www.sigmaaldrich.com). 1,3,5-Trimesic acid was obtained from Shang Hai Yuanye Biology (http://www.shyuanye.com). L(+)-Ascorbic acid was supplied by Guangdong Guanghua Sci-Tech Co., Ltd. $NaBH_4$, H_2O_2, NaCl, KCl were purchased from Chongqing Chuandong Chemical Group (Co. Ltd, Chongqing, China). Polyvinylpyrrolidone (PVP) was obtained from Sangon (http://www.sangon.com). Bovine serum albumin (BSA), gold (III) chloride trihydrate ($HAuCl_4{\cdot}3H_2O$) and Ruthenium(III) chloride anhydrous were all purchased from Aladdin (Shanghai, China, www.aladdin-e.com). The real samples were provided by University-Town Hospital of Chongqing Medical University (Chongqing, China). The DNA oligonucleotides described in Table S1 were synthesized and purified by Sangon Biotechnology, Inc. (Shanghai, China). Human Elisa kit of Thrombospondin-1(TSP-1) was supplied by Assay.

The stock solutions of all of the oligonucleotides were prepared with 1 × TE buffer (10 mM, trishydroxymethylaminomethane hydrochloride (Tris-HCl) and 1.0 mM ethylenediaminetetraacetic acid (EDTA), pH 8.0). The other buffer was listed in Table S1. All other reagents were of analytical reagent grade and were used directly without further purification. Milli-Q water (> 18.2 MΩ) obtained from a Millipore Mill-Q purification system was used throughout the experiments.

2.2. Apparatuses

The details are provided in Supplementary information (S1).

2.3. Preparation of Ce-MOF@Au nanocomposite

Ce-MOF were synthesized according to the literature (Yuhao et al., 2015). Then, gold nanoparticles were synthesized on the Ce-MOF surface by in situ reduction as shown in Scheme 1A. First, Ce-MOF (1 mg) was dispersed in Milli-Q water (2 mL), and then 2% $HAuCl_4$ (2 mL) was added. After mixing well, a PVP solution (2 mL, 2 mg mL^{-1}) was added followed by ultrasonic mixing for 15 min. After stirring at 800 rpm, $NaBH_4$ (2 mL, 7.5 mg mL^{-1}) was slowly added dropwise. The mixture was stirred at room temperature for 30 min, centrifuged, washed with Milli-Q water (2 mL) three times to obtain a Ce-MOF@Au nanocomposite, and dispersed in Milli-Q water for further use.

2.4. Preparation of AuPtRu, AuPt, AuRu and PtRu nanocomposite

In this study, AuPtRu NPs were prepared by ascorbic acid reduction at 4 °C. Briefly, $RuCl_3$ (0.9 mL, 20 mM), 5% $HAuCl_4$ (53.2 μL), 5% H_2PtCl_6 (88.4 μL), and Pluronic F127 (0.01 g) were placed in a beaker and mixed. Then, ascorbic acid (AA) (0.3 mL, 0.4 M) was gradually added with stirring (800 rpm) at 4 °C. After 3 h, the mixture was centrifuged and washed three times, and the centrifuged product was dispersed in Milli-Q water (500 μL).

AuPt, AuRu and PtRu nanocomposites were synthesized by a similar method, except that 20 mM $RuCl_3$ (0.9 mL) was displaced by H_2O (0.9 mL), 5% H_2PtCl_6 (88.4 μL) was displaced by H_2O (88.4 μL) and 5% $HAuCl_4$ (53.2 μL) was displaced by H_2O (53.2 μL). The synthesized products were dissolved in Milli-Q water (500 μL).

2.5. Preparation of AuPtRu/S1 (SP, signal probe)

As shown in Fig. 1A, this part of the experiment was performed in an Eppendorf tube. First, 4 μM S1 and 4 μM aptamer were mixed in equal volumes, heated at 90 °C for 10 min, and then cooled to room

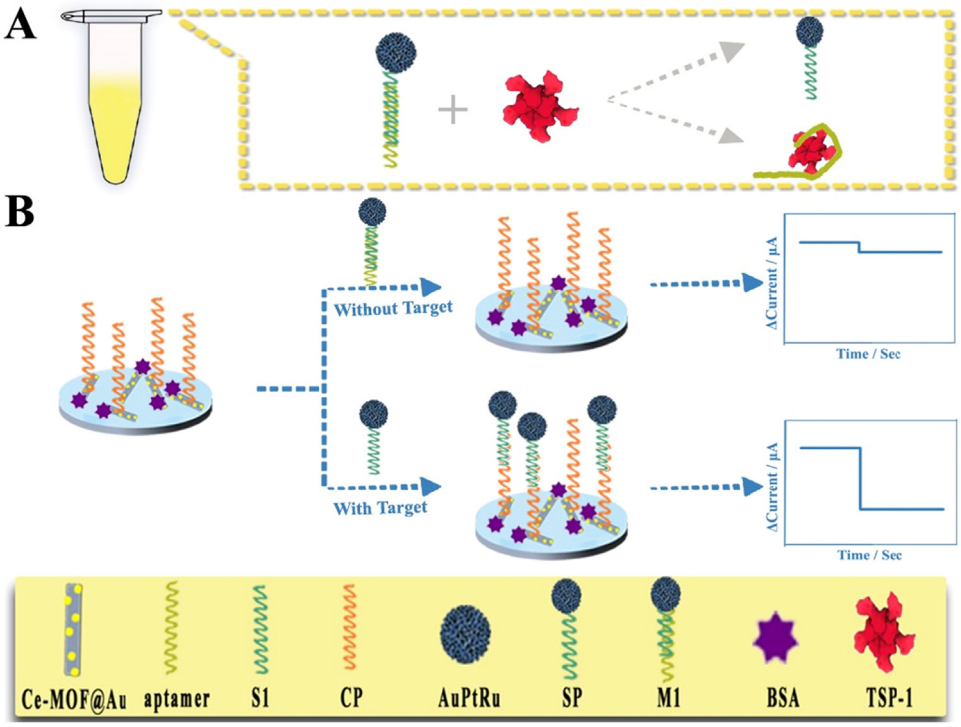

Scheme 1. Schematic illustration of the assembly procedure of the electrochemical biosensor. A: Preparation of AuPtRu/S1 (SP, signal probe) in Eppendorf tube. B: Construction of the aptasensor.

temperature for 1 h to obtain partially hybridized M1 (SP + aptamer double strand). Hybridized double strands (200 μL) were added to the AuPtRu trimetal mixed solution (1 mL) and shaken at 4 °C for 12 h. The mixture was centrifuged (8000 rpm) and washed once with Milli-Q water, and dissolved in the hybridization solution (1 mL). 0.5% BSA was added so that the nonspecific binding site was blocked. Then, the mixture was shaken at 4 °C for 2 h, centrifuged again (2000 rpm) and washed once with Milli-Q water, and dispersed in the Milli-Q water (1 mL). Finally, different concentrations of TSP-1 (200 μL) were added to the mixed liquid obtained as described above, so that the SP in the M1 (SP + aptamer double strand) was released and an electrochemically active SP was obtained.

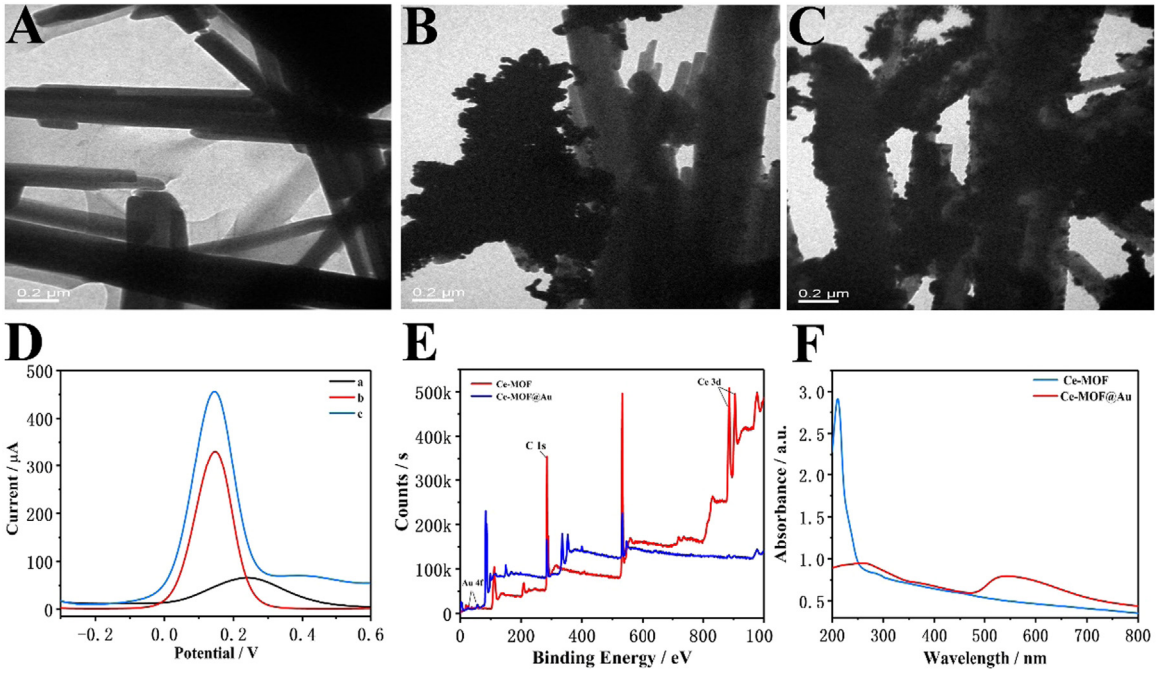

Fig. 1. TEM images of (A) Ce-MOF, (B) Ce-MOF@Au (Method 1), (C) Ce-MOF@Au (Method 2). (D) DPV for the comparison of electrochemical performance of Ce-MOF@Au obtained by two synthetic methods (a) GCE; (b) synthesis of Ce-MOF@Au by Method 1; (c) synthesis of Ce-MOF@Au by Method 2 (E) XPS spectrum of Ce-MOF and Ce-MOF@Au. (F) UV–visible absorption of Ce-MOF@Au.

2.6. Construction of aptasensor

The fabrication of the electrochemical biosensor is outlined in Scheme 1B. Prior to the modification, the GCE was polished sequentially on the suede with 0.3 and 0.05 μm alumina powder, and then the electrode was sonicated with absolute Milli-Q water, ethanol and Milli-Q water for 3 min in an ultrasonic bath in order to remove the remaining absorbed particles. Thus, a smooth interface was obtained. After the electrode was dried at room temperature, the prepared Ce-MOF@Au nanocomposite was modified onto a GCE, and then 4 μM CP solution (10 μL of) was added to incubate at 4 °C overnight. The CP was immobilized through Au-NH_2 bonds. Finally, to block the active vacancies, a 0.5% BSA solution was incubated at room temperature for 30 min. After washing, the fabricated electrode was stored at 4 °C for further use.

2.7. Measurement procedure

10 μL prepared SP was added to the surface of the GCE/Ce-MOF@Au/CP/BSA electrode prepared and incubated for 2 h at 37 °C. After the reaction, the electrode was washed with Milli-Q water to remove unbound conjugates. To perform the electrochemical analysis, the amperometric i-t curves were obtained at − 0.4 V in PBS (5 mL, pH 7.0)·H_2O_2 (20 μL, 2.2 mol L^{-1}) was added into the PBS under on-going stirring (300 rpm) when the background current was stable, and changes in the response current were recorded.

3. Results and discussion

3.1. Ce-MOF characterization

Ce-MOF morphology was characterized by TEM. As was shown in Fig. 1A, Ce-MOF has a long rod structure with the length of 4 ~ 5 μm and the width of 300 ~ 400 nm, which was consistent with the literature (Xiong et al., 2015). The XRD of Ce-MOF was shown in Fig. S1. The results showed that Ce-MOF was synthesized successfully.

3.2. Choice of the Ce-MOF@Au synthesis method

As described above, in order to solve the problem of easy aggregation of Au NPs during in-situ reduction, PVP was added as a protective agent (Xiao et al., 2012). At the same time, we explored that whether the addition order of PVP during the synthesis process will affected the morphology and electrochemical characteristics of Ce-MOF@Au. Therefore, two methods were designed to verify a proper PVP addition order. In Method 1, the PVP was added prior to the addition of chloroauric acid, while PVP was added after the addition of chloroauric acid in Method 2. The morphological and electrochemical properties of Ce-MOF@Au obtained by the two methods were verified by transmission electron microscopy (TEM) and differential pulse voltammetry (DPV). As shown in Fig. 1B, Au NPs were successfully reduced to the Ce-MOF surface by Method 1. Excessive Au NPs were present on some rod-shaped Ce-MOF while there were no Au NPs on some of the Ce-MOF. When Ce-MOF@Au was obtained by Method 2, the Au NPs reduced to the surface of Ce-MOF more uniformly (Fig. 1C). Next, DPV was used to evaluate the electron transfer capability of the Ce-MOF@Au obtained by each of the two methods (Fig. 1D). Comparison of Method 1 with Method 2 shows that the obtained Ce-MOF@Au nanocomposites have significantly better electron conductivity when PVP is added after the addition of chloroauric acid. Therefore, PVP added after Ce-MOF and $HAuCl_4$ were mixed, which is beneficial to the sufficient contact of Ce-MOF with $HAuCl_4$, and can be distributed more uniform distribution on the Ce-MOF surface after Au NP reduction. We chose Method 2 to synthesize Ce-MOF@Au for subsequent experiments.

3.3. Characterization of Ce-MOF@Au

The composition of Ce-MOF@Au was studied further by XPS (Fig. 1E). The peak of carbon (C) element was present on the XPS image of Ce-MOF, and a distinct of Ce element peak appears around 890 eV (Yuhao et al., 2015). When the Ce-MOF@Au complex was formed, it was observed that a characteristic peak of Au NPs appeared. At the same time, the characteristic peaks of element C and Ce of Ce-MOF@Au appear to be greatly attenuated. This is because the Au NPs were wrapped on the surface of Ce-MOF, which indicates the synthesis of Ce-MOF@Au. Next, UV–vis spectroscopy was used to verify the presence of Au NPs (Fig. 1F). Ce-MOF has a distinct absorption peak near 210 nm that is due to the π-π * transition of benzene in the organic ligand trimesic acid of synthetic MOF (Arivazhagan and Rexalin, 2013; Khan and Khan, 2005). A distinct characteristic absorption peak of Au can be observed in Ce-MOF@Au, while Ce-MOF had no obvious UV absorption peak at 520 nm (Perrault and Chan, 2009). At the same time, the intensity of the peak near 210 nm has drastically decreased because Au NPs covered the surface of the Ce-MOF. This comparison showed that there were Au NPs presented on the Ce-MOF surface. As was shown in Fig. S2, the formation of Ce-MOF@Au was further confirmed by FE-SEM, EDS and ζ-potential measurement. Fig. S2A and S2B showed a clear presence of Au NPs on the surface of the rod Ce-MOF. EDS results (Fig. S2C) showed the presence of the Ce and Au elements. Furthermore, the change in the potential was monitored by the ζ-potential. Fig. S2D shows that the Ce-MOF and Ce-MOF@Au potentials were 1.42 and −3.93, respectively. The potential changes from positive to negative because the PVP-protected Au NPs were negative and when Au NPs were reduced to the Ce-MOF, the potential became negative (Wang et al., 2016). The electrochemical properties of Ce-MOF@Au were measured and are shown in Fig. S3. Cyclic voltammograms (CV, Fig. S3A) and electrochemical impedance spectroscopy (EIS, Fig. S3B) showed that Ce-MOF@Au had a better conductivity than Ce-MOF due to the presence of Au NPs. Based on these results, it was confirmed that Ce-MOF@Au has been successfully synthesized.

3.4. Characterization and catalytic performance comparison of AuPtRu nanosphere

The structure, morphology and size of AuPtRu NPs were characterized by FE-SEM (Fig. 2A-D). As observed from these figures, AuPtRu NPs showed a line-like globular structure with uniform distribution and no aggregation, and the average diameter of the nanospheres was approximately 500 nm. ζ-potential was used to verify the synthesis and stability of AuPtRu NPs. Fig. 2E showed that the synthesis of AuPtRu NPs cause an obvious potential change compared to the potentials of Au NPs, Pt NPs and bimetallic AuPt. As we know, an increase in the absolute value of the material potential means a better stability of material. The absolute value of the AuPt bimetal was greater than the single metal constituting it, and the absolute value of the AuPtRu trimetal was greater than AuPt bimetal. This was attribute to Ru not only has the ability to catalyze H_2O_2, but also has the effect of stabilizing AuPt NPs. Meanwhile, AuPtRu NPs was successfully synthesized. Three kinds of bimetallic nanomaterials (AuPt, AuRu and PtRu) were synthesized by the same method, and their catalytic properties were compared with AuPtRu NPs by i-t curves. Fig. 2F shows that AuPtRu NPs exhibited more superior catalytic performance. These results show that the AuPtRu NPs with excellent catalytic and stability have been successfully synthesized.

Specific coupling was studied by agarose gel electrophoresis among CP, S1, aptamer, TSP-1 and mixture of CP + S1 + aptamer + TSP-1. In Fig. S4, lane a was 20 bp marker, and lanes b and c were S1 and CP, respectively. Lane c displayed the highest mobility because of its lowest molecular weight. S1-CP conjugate (lane d) showed lower mobility compared to S1 and CP, indicating that SP and CP hybridized successfully. Lane e was the aptamer and lane f was the CP-aptamer

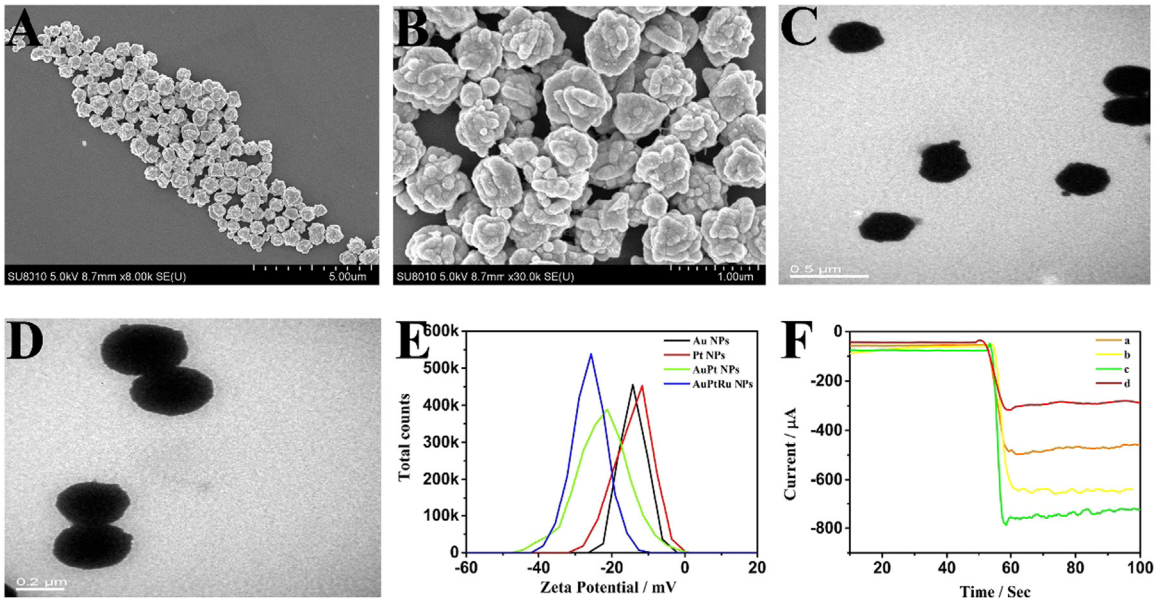

Fig. 2. (A) and (B) FE-SEM image of AuPtRu; (C) and (D) TEM image of AuPtRu; (E) ζ-potential comparison of Au, Pt, AuPt and AuPtRu; (F) i-t curve characterization of the catalytic ability of (a) AuPt; (b) AuRu; (c) RuPt; (d) AuPtRu.

conjugate, and it was observed that there was no significant mobility change due to the inability of CP to hybridize to aptamer. Lane g (S1 + aptamer) has a lower mobility than aptamer (lane e), which confirms that S1 and aptamer can be successfully hybridized. The results above confirmed the feasibility of hybridization.

3.5. Morphology and electrochemical performance of modified electrodes

AFM was used to morphologically characterize the electrode construction process, as is shown in Fig. 3. As observed from Fig. 3A, some small particles were present on the surface of Ce-MOFs@Au. The surface roughness increased from 23.3 nm to 48.2 nm after incubating with CP (Fig. 3B), indicating that CP was successfully immobilized on Ce-MOFs@Au. When BSA was incubated, the surface roughness was

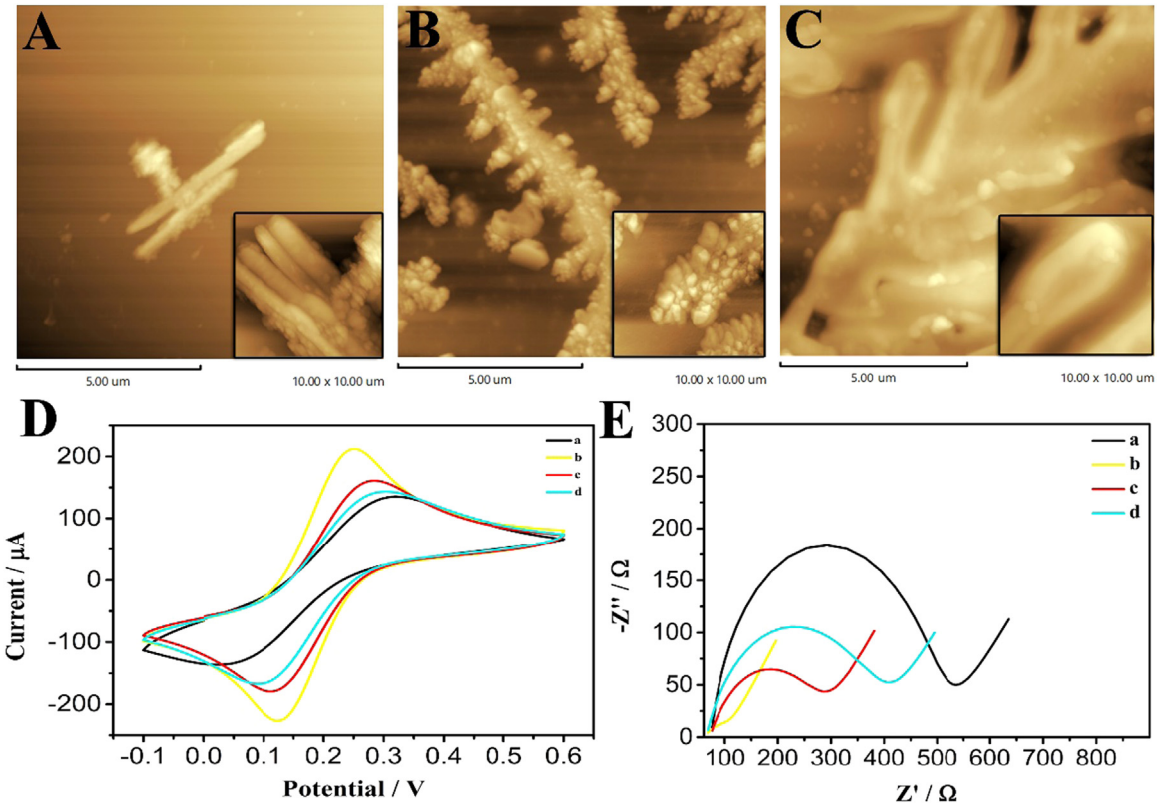

Fig. 3. AFM results for (A) Ce-MOF@Au, (B) Ce-MOF@Au/CP, (C) Ce-MOF@Au/CP/BSA; (D) CV and (E) EIS characterization of the electrodes at various steps of modification in a 5 mM $[Fe(CN)_6]^{3-/4-}$ solution: (a) bare GCE, (b) GCE/Ce-MOF@Au, (c) GCE/Ce-MOF@Au/CP, (d) GCE/Ce-MOF@Au/CP/BSA.

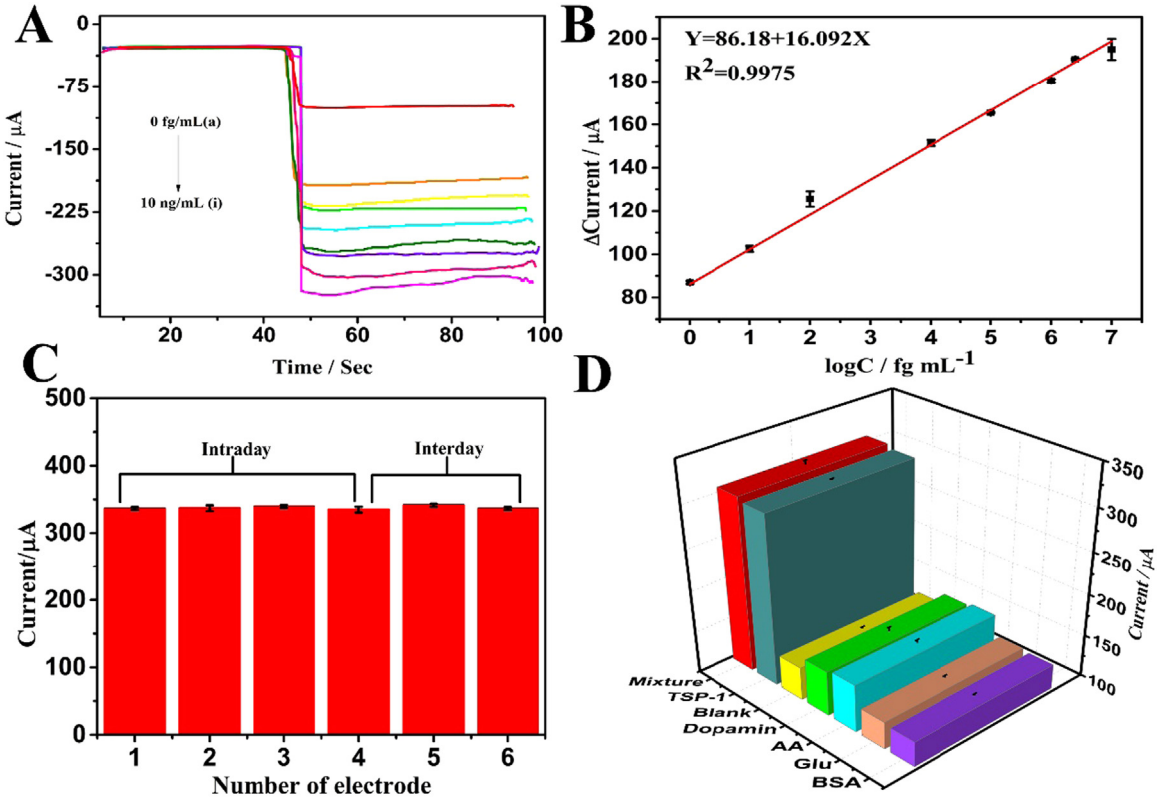

Fig. 4. (A) i-t curves for the proposed aptasensor with different target DNA concentrations in 5 mL of PBS (pH 7.4) with the addition of H_2O_2 (2.2 mol L^{-1}). (B) Calibration curve of the aptasensor for different concentrations of target DNA (a-q: 0–10 ng mL^{-1}). (C) Reproducibility of different electrodes modified with 100 pg mL^{-1} of TSP-1. (D) Specificity of the aptasensor investigated with blank control, 1 ng mL^{-1} dopamine, 1 ng mL^{-1} AA, 1 ng mL^{-1} glucose, 1 ng mL^{-1} BSA, 100 pg mL^{-1} TSP-1 and the related mixture.

decreased to 39.6 nm (Fig. 3C), because the gap between Ce-MOF@Au/CP was full of BSA. The AFM results successfully provided the morphological characterization of the electrode construction process.

For the electrochemical characterization, CV was employed to verify the fabrication process of the aptasensor. As shown in Fig. 3D, compared to the bare GCE (curve a), the redox peak current showed a significant increase when Ce-MOF@Au was modified on the GCE. This was attributed to the excellent electron transfer ability of Ce-MOF@Au as the electrode modification material. When the electrode was further loaded with the CP decorated with amino group due to the Au-NH_2 bond, a decreased peak current was observed (curve c). This was mainly due to the weak conductivity of DNA which hinders the electron transfer. With the BSA assembled on the electrode, the CV response of the electrode decreased further (curve d). The modification steps were also characterized by EIS in 5 mM $[Fe(CN)_6]^{3-/4-}$ and 0.1 M KCl (Fig. 3E). The diameter of the semicircle in EIS is related to the charge transfer resistance (Ret). The EIS results are in agreement with the CV data, confirming the successful construction of the aptasensor.

3.6. Optimization of experimental conditions

To obtain the best experimental conditions, the concentration of Ce-MOF@Au, the incubation time of CP, the pH of PBS, the binding time of M1(SP + aptamer double strand) to target protein TSP-1, and the concentration of H_2O_2 were optimized because these factors affected the performance of the constructed aptasensor.

The amount of the modifying material Ce-MOF@Au on the electrode directly affected the electron transfer capability of the electrode, therefore, the concentration of Ce-MOF@Au was investigated in the range of 0.625–10 mg mL^{-1}. It is observed from Fig. S5A that when the concentration of Ce-MOF@Au ranged from 0.625 mg mL^{-1} to 4 mg mL^{-1}, the current response value gradually increased and reached a maximum at the concentration of 4 mg mL^{-1}. As the concentration increased further, the current value tended to be stable. Therefore, 4 mg mL^{-1} was chosen as the modified concentration of Ce-MOF@Au.

Fig. S5B shows the relationship of the peak current versus the incubation time of the capture probe in the range of 8 ~ 16 h. Since the incubation time of CP was in the range of 8 ~ 12 h, the peak current decreased gradually, and when the incubation time reached 12 h, the peak current drop value is maximized implying that the number of CP bonded to the electrode surface is maximized. In the range of 12 ~ 16 h, the peak current no longer increased, indicating that the reaction tended to be saturated. Therefore, 12 h was chosen as the optimal incubation time for CP.

The binding time of M1 to target protein TSP-1 is an important parameter in the construction of the aptasensor (Fig. S5C). When M1 and TSP-1 were combined between 1 ~ 2.5 h, the peak current was significantly increased. After further incubation, the current had not continued to rise. Therefore, M1 and TSP-1 should be combined for 2.5 h.

Since the H_2O_2 concentration directly affected the measurement results, it was necessary to be optimized. Fig. S5D shows that the concentration of the added H_2O_2 in the range of 1.8 mol ~ 2.2 mol L^{-1}, the peak current showed a significant increase, and then upon a further increase in the concentration of H_2O_2, the peak current tends to be stable. Therefore, 2.2 mol L^{-1} was chosen as the H_2O_2 concentration for this experiment.

As shown in Fig. S5E, the current peak of the aptasenser changed as the pH value changed between 6.0 and 8.0. Moreover, the oxidation current of the aptasensor reached the maximum value at pH 7.0. Therefore, pH 7.0 was chosen for this work.

Table 1
Comparison of the relevant TSP-1 detection methods.

Detection	Recognition elements	Linear range	Detection limit	Ref.
ELISA	antibodies	7.8 ng mL^{-1}–500 ng mL^{-1}	0.944 ng mL^{-1}	–
Electrochemistry	aptamer	5 fM − 100 fM	6.69 fM	(Ji et al., 2014)
Electrochemistry	aptamer	1 fg mL^{-1}–10 ng mL^{-1}	0.13 fg mL^{-1}	This work

3.7. Analytical performance of the aptasensor

The analytical performance of the aptasensor for detecting TSP-1 was studied for a series of TSP-1 concentrations using an i-t curve under optimal conditions. The amperometric i-t curve was determined by adding H_2O_2 (20 μL, 2.2 mol L^{-1}) to PBS (5 mL, 0.1 M, pH 7.4). As shown in Fig. 4A, due to the specific binding between the aptamer and TSP-1, the current response gradually increases with the TSP-1 concentration increasing from 1 fg mL^{-1} to 10 ng mL^{-1}. As shown in Fig. 4B, the detected current change had a good linear relationship with the logarithm values of the TSP-1 concentrations. The linear regression equation $Y = 86.18 + 16.092 \times$, with the correlation coefficient of 0.9975 and the detection limit of 0.13 fg mL^{-1} ($LOD = 3S_B/m$ (Bai et al., 2012)). The results show that the constructed aptasensor can be used for the quantitative detection of TSP-1. Trimetallic signal amplification aptasensor exhibits an extremely low detection limits for the following reasons: first, high specificity and strong affinity between the aptamer and TSP-1; second, Ce-MOF@Au has excellent electron conductivity; finally, the AuPtRu NPs have excellent catalytic ability for H_2O_2. The aptasensor was compared to other methods for TSP-1 assay and the results are listed in Table 1. The comparison clearly showed that the proposed aptasensor achieved better performance at lower detection limits.

3.8. Specificity, reproducibility and stability

The reproducibility of the aptasensor was investigated by evaluating i-t responses (Fig. 4C). By detecting the same concentration of TSP-1(100 pg mL^{-1}), the relative standard deviation (RSD) of the intra-assay and inter-assay of the TSP-1 aptasensor were 0.91% and 0.99% respectively, implying the superior reproducibility of the proposed TSP-1 aptasensor for potential practical applications.

Since specificity is the basis of sensor applications, the specificity of the constructed aptasensor was evaluated. As shown in Fig. 4D, several 1 ng mL^{-1} nontarget interfering substances including AA, BSA, glucose and dopamine were tested. All of the nontarget substances were not detected with significant signal values compared to the blanks. In addition, the constructed aptasensor was incubated with 100 pg mL^{-1} TSP-1 containing all of the above interfering substrate mixtures, and no significant difference was observed compared to the current obtained from only 100 pg mL^{-1} TSP-1, indicating that the proposed aptamer sensor has good specificity.

The aptasensor stability was investigated by an amperometric i-t curve in the presence of TSP-1 (100 pg mL^{-1}). The prepared aptasensors were stored under the same conditions at 4 °C when not in use. After the first 7 days, the detection results decreased by less than 0.3%. A decrease in the current response of 6.4% was observed after 21 days. After storage for 30 days, the catalytic activity was maintained at 91.60%. The observed slight decrease may be due to the long-term storage of biologically active molecules leading to inactivation. The results show that the aptasensor has excellent stability.

3.9. Analysis of TSP-1 in real human serum samples

To evaluate the detection accuracy of the aptasensor, the recovery rate was tested. As observed from the data presented in Table S3, we detected responses to different concentrations of TSP-1 (10 fg mL^{-1}, 100 pg mL^{-1}, 2.5 ng mL^{-1}) added to 10-fold diluted human serum samples. The recovery rate was acceptable which was ranged from 93.29% to 108.28%.

3.10. Analysis of TSP-1 in real samples

To further evaluate the potential of aptasensors in clinical applications, the feasibility and accuracy were tested by detecting 10-fold diluted real serum samples from actual myocardial infarction patients, hypertensive patients and healthy people. At the same time, the same actual samples were analyzed by ELISA. Comparing the results obtained by the two methods, Table S4 shows that the relative error of the present method was 0.1–7.80%. Additionally, as shown in Fig. S6, the concentrations of TSP-1 for normal people and patients were significantly different (< 0.001). The test results for the real samples were consistent with the ELISA test results, and the TSP-1 levels of the patients with cardiovascular disease were higher than normal, proving that TSP-1 may be a potential marker for the diagnosis of myocardial infarction and hypertension. The results also showed that the aptasensor can be effectively applied to the determination of TSP-1 in real human serum.

4. Conclusion

In summary, we designed a trimetallic signal amplification strategy based on Ce-MOF@Au and AuPtRu NPs, aptamer recognizes TSP-1 and nucleic acid single-stranded complement recognition as a bispecific recognition mechanism for sensitive detection of TSP-1. First, Ce-MOF@Au was prepared by an in-situ reduction method, and electrical signal amplification was obtained by enhancing the conductivity of the electrode in the aptasensor. Second, the AuPtRu trimetallic nanocomposite was synthesized, and introduced into the aptamsensor as a catalytic signal amplification material and nucleic acid immobilization material. Finally, the nucleic acid single-strand complementation, the high specificity and high affinity between the aptamer and the target substance, as the recognition mechanism. With this dual signal amplification, the proposed aptasensor shows an extremely high sensitivity to TSP-1 detection. In addition, we suggest that our approach is expected to have great potential for the auxiliary diagnosis of various diseases caused by TSP-1.

CRediT authorship contribution statement

Xiaoxue Fu: Conceptualization, Data curation, Formal analysis, Investigation, Methodology, Validation, Writing - original draft. **Junlin He:** Conceptualization, Data curation, Formal analysis, Investigation, Methodology, Validation, Writing - original draft. **Chengli Zhang:** Conceptualization, Formal analysis. **Jun Chen:** Conceptualization, Formal analysis. **Yilin Wen:** Methodology, Visualization. **Jia li:** Methodology, Visualization. **Weiran Mao:** Methodology, Visualization. **Hangtian Zhong:** Methodology, Visualization. **Jiahao Wu:** Methodology, Visualization. **Xingduo Ji:** Methodology, Visualization. **Chao Yu:** Funding acquisition, Resources, Supervision, Writing - review & editing.

Acknowledgments

We are grateful for the financial support from the National Nature Science Foundation of China (No. 81370403), Chongqing foundation and advanced research project (No. CSTC2015jcyjBX0053), Chongqing precision medical key technology research and development and demonstration projects (cstc2016shms-ztzx0042), Chongqing medical university scientific research cultivating fund (No. 201414) and outstanding graduate student cultivation program of Chongqing Medical University (BJRC201830).

Declaration of interest statement

None.

Appendix A. Supplementary material

Supplementary data associated with this article can be found in the online version at doi:10.1016/j.bios.2019.02.054.

References

Arivazhagan, M., Rexalin, D.A., 2013. Spectrochim. Acta A Mol. Biomol. Spectrosc. 107, 347–358.
Bai, L., Chen, Y., Bai, Y., Chen, Y., Zhou, J., Huang, A., 2017. Biomaterials 133, 11–19.
Bai, L., Yuan, R., Chai, Y., Zhuo, Y., Yuan, Y., Wang, Y., 2012. Simultaneous electrochemical detection of multiple analytes based on dual signal amplification of single-walled carbon nanotubes and multi-labeled graphene sheets. Biomaterials 33, 1090–1096.
Campbell, M.G., Sheberla, D., Liu, S.F., Swager, T.M., Dinca, M., 2015. Angew. Chem. Int Ed. Engl. 54, 4349–4352.
Chavez, R.J., Haney, R.M., Cuadra, R.H., Ganguly, R., Adapala, R.K., Thodeti, C.K., Raman, P., 2012. Am. J. Physiol. Cell Physiol. 303, C179–C191.
Christensen, S.T., Feng, H., Libera, J.L., Guo, N., Miller, J.T., Stair, P.C., Elam, J.W., 2010. Nano Lett. 10, 3047.
Chuanfu, X., Shoumin, C., Laiying, Z., Shuiqin, Z., Weitai, W., 2012. Chem. Commun. 48, 11751–11753.
Cui, J.W., Luo, J.B., Peng, B.G., Zhang, X.Y., Zhang, Y., Wang, Y., Qin, Y.Q., Zheng, H.M., Shu, X., Wu, Y.C., 2016. 8, 770–774.
Dang, S., Zhu, Q.-L., Xu, Q., 2017. Nat. Rev. Mater. 3, 17075.
Du, Y., Chen, C., Yin, J., Li, B., Zhou, M., Dong, S., Wang, E., 2010. Anal. Chem. 82, 1556–1563.
Eid, K., Malgras, V., He, P., Wang, K., Aldalbahi, A., Alshehri, S.M., Yamauchi, Y., Wang, L., 2015. RSC Adv. 5, 31147–31152.
Feng, L., Chen, Y., Ren, J., Qu, X., 2011. Biomaterials 32, 2930–2937.
Gao, F., Du, L., Zhang, Y., Zhou, F., Tang, D., 2016. Biosens. Bioelectron. 86, 185–193.
Hong, W., Wang, J., Wang, E., 2015. J. Mater. Chem. A 3, 13642–13647.
Ji, K., de Carvalho, L.P., Bi, X., Seneviratnankn, A., Bhakoo, K., Chan, M., Yau Li, S.F., 2014. Biosens. Bioelectron. 55, 405–411.
Kang, S.W., Lee, Y.W., Park, Y., Choi, B.S., Hong, J.W., Park, K.H., Han, S.W., 2013. Acs Nano 7, 7945–7955.
Khan, M.S., Khan, Z.H., 2005. Spectrochim. Acta Part A Mol. Biomol. Spectrosc. 61, 777–790.
Li, H.H., Zhao Prof., #x, S., Gong, D.M., Cui, C.H., He, D., Liang, H.W., Wu Prof., #x, L., Yu, D.S.-H., 2013. Angew. Chem. 52, 7472–7476.
Li, P.Z., Wang, X.J., Tan, S.Y., Chen, H.Z., Liu, J., Zou, R.Q., Zhao, Y.L., 2015. Angew. Chem. Int. Ed. 54, 12748–12752.
Li, Q., Yu, C., Gao, R., Xia, C., Yuan, G., Li, Y., Zhao, Y., Chen, Q., He, J., 2016. Biosens. Bioelectron. 80, 674–681.
Nguyen, T.T., Wu, K.Y., Leclerc, M., Pham, H.M., Tran, S.D., 2018. Current oral. Health Rep. 5, 13–18.
Pei, F., Wang, P., Ma, E., Yu, H., Gao, C., Yin, H., Li, Y., Liu, Q., Dong, Y., 2018. Biosens. Bioelectron.
Perrault, S.D., Chan, W.C., 2009. J. Am. Chem. Soc. 131, 17042–17043.
Salajegheh, A., 2016.
Shen, W.J., Zhuo, Y., Chai, Y.Q., Yuan, R., 2016. Biosens. Bioelectron. 83, 287–292.
Tang, Z., He, J., Chen, J., Niu, Y., Zhao, Y., Zhang, Y., Yu, C., 2018. Biosens. Bioelectron. 101, 253–259.
Wang, L., Ma, R., Jiang, L., Jia, L., Jia, W., Wang, H., 2016. Biosens. Bioelectron. 92, 390–395.
Wang, Y., Li, Y., Sun, G., Zhang, G., Liu, H., Du, J., Yang, S., Bai, J., Yang, Q., 2010. J. Appl. Polym. Sci. 105, 3618–3622.
Xiao, C., Chen, S., Zhang, L., Zhou, S., Wu, W., 2012. Chem. Commun. 48, 11751–11753.
Xiong, Y.H., Chen, S.H., Ye, F.G., Su, L.J., Zhang, C., Shen, S.F., Zhao, S.L., 2015. Chem. Commun. 51, 4635–4638.
You, H., Bai, L., Yuan, Y., Zhou, J., Bai, Y., Mu, Z., 2018. Biosens. Bioelectron. 117, 706–712.
Yuhao, X., Siheng, C., Fanggui, Y., Lingjing, S., Cong, Z., Shufen, S., Shulin, Z., 2015. Chem. Commun. 51, 4635–4638.
Yusuf, S., Reddy, S., Ounpuu, S., Anand, S., 2001. Circulation 104, 2746–2753.
Zeng, D., Zhang, H., Zhu, D., Li, J., San, L., Wang, Z., Wang, C., Wang, Y., Wang, L., Zuo, X., 2015. Biosens. Bioelectron. 71, 434–438.
Zhang, E., Xie, Y., Ci, S., Jia, J., Wen, Z., 2016. Biosens. Bioelectron. 81, 46–53.
Zhu, H., Zhang, S., Guo, S., Su, D., Sun, S., 2013. J. Am. Chem. Soc. 135, 7130–7133.